Astron. Astrophys. 336, 840–854 (1998)

ASTRONOMY AND ASTROPHYSICS

Stellar disks of optically flocculent and grand design spirals⋆

Decoupling of stellar and gaseous disks

P.J. Grosbøl[1] **and P.A. Patsis**[2,3]

[1] European Southern Observatory, Karl-Schwarzschild-Str. 2, D-85748 Garching, Germany
[2] Max-Planck Institut für Astronomie, Königstuhl 17, D-69117 Heidelberg, Germany
[3] Astronomisches Rechen Institut, Mönchhofstraße 12-14, D-69120 Heidelberg, Germany

Received 24 March 1998 / Accepted 8 June 1998

Abstract. Accurate surface photometry of five spiral galaxies (NGC 3223, NGC 5085, NGC 5247, NGC 5861 and NGC 7083) in visual and near-infrared bands is presented. All galaxies show grand design spiral structure in K′ although several have a flocculent appearance on blue images suggesting that stellar and gaseous disks are decoupled. The decomposition of the K′ maps in axisymmetric components suggests that both a spherical bulge and a flat exponential disk are required to explain the light distribution in the bulge regions. The central disk has a short scale length and sky projection parameters similar to the main disk. The scale length of the main exponential disk measured in the interarm region is consistently smaller than the value determined from the arms for three of the galaxies. Weak oval distortions were found in three galaxies while only one was classified as such. The galaxies with oval distortions have less concentrated and fainter bulges than those in the two galaxies without such ovals.

Model rotation curves were constructed for each galaxy based on the axisymmetric decomposition of their K′ surface brightness maps and observed velocity data. The mass-to-light ratio estimated in K′ for the disk component was around 0.7 in solar units for all galaxies using the disk scale length derived from the interarm regions.

Pitch angles of the main two-armed spiral estimated in B,V,I and K′ show a systematic trend of arms being tighter in bluer colors which suggests the presence of density waves in the galaxies. Comparing the extent of the spiral pattern in the galaxies with their angular velocity curves, the best agreement was obtained when the symmetric, two-armed spiral starts just outside ILR and terminates around the 4:1 resonance. The spirals continue beyond this region but are weaker and more fragmented. The pattern speed estimated for the two Sb galaxies was significantly higher than that for the Sc galaxies.

Several galaxies have dust spirals inside the main stellar spiral. In most cases, the main spiral pattern is more open in the inner region than further out where it is well approximated with a logarithmic spiral. This may support a scenario where a central oval distortion drives the spiral, which then would correspond to the long waved solution of the dispersion relation.

Key words: galaxies: kinematics and dynamics – galaxies: photometry – galaxies: spiral – galaxies: structure – infrared: galaxies

1. Introduction

The large scale spiral arms observed in disk galaxies may in many cases be explained as density waves (Lin & Shu 1964) in their old stellar population. Near-infrared images of spiral galaxies (e.g. Block & Wainscoat 1991; Rix & Rieke 1993; Block et al. 1994; Block et al. 1996) show smooth, symmetric arms in their disks supporting the existence of density waves. Several important properties related to the dynamic nature of such waves cannot be determined directly and are therefore still poorly known e.g. their pattern speed, excitation and lifetime. Density waves could either be relative short lived phenomena consisting of single wave packages traveling through the disk (Toomre 1969, 1981) after e.g. an encounter, or be standing waves in the framework of the modal theory (Bertin et al. 1989a,b) with a much longer life. Waves excited by oval distortions in the center (Schwarz 1981; Schempp 1982) could also exist over a long time span.

An important tool to distinguish between different scenarios and estimate dynamic parameters is a detailed comparison between observations of galaxies and models. In the visual, several studies have been made (see e.g. Schweizer 1976; Patsis et al. 1991) but uncertainties in the correction for dust extinction and lack of accurate kinematic data made the interpretation difficult. Radio observations of gas kinematics (see e.g. Visser 1980; Canzian & Allen 1997) provide important information on the dynamics of density waves but are limited by resolution. The interpretation of such observations is complex as it depends on the state of the gas in the galaxies.

Direct observations of density perturbations associated to spiral arms in galaxies are difficult due to strong correlation between dust and population effects in arm regions which cannot be disentangled reliably using broad band colors (Witt et al.

Send offprint requests to: P.J. Grosbøl,(pgrosbol@eso.org)

⋆ Based on observations collected at the European Southern Observatory, La Silla, Chile

Table 1. List of galaxies observed. The morphological type and corrected recession velocity taken from RSC are given in addition to the diameter D_{25} and axis ratio R_{25} from RC3. The linear scale adopted is also listed.

	RSC		RC3		scale
Galaxy	Type	v_0 (km/s)	D_{25}	R_{25}	(pc/″)
NGC 3223	Sb(s)I-II	2619	4′.1	1.66	169.3
NGC 5085	Sc(r)I-II	1720	3′.4	1.15	111.2
NGC 5247	Sc(s)I-II	1143	5′.6	1.15	73.9
NGC 5861	Sc(s)II	1725	3′.0	1.82	111.5
NGC 7083	Sb(s)I-II	2951	3′.9	1.66	190.8

1992). The effects of dust extinction decrease with wavelength but is still significant in the J and H bands. The attenuation of dust first becomes negligible in normal spiral galaxies in the K-band at 2.2μm. Near-infrared (NIR) bands are also more sensitive to the old stellar disk population than to young objects and will therefore better trace the mass distribution (Rix 1993). Developments of NIR array detectors have made deep, accurate surface photometry in K possible and thereby opened for detailed studies of the morphology of density variations in galactic disks.

The current paper presents accurate visual and NIR surface photometry of 5 ordinary spirals and analyzes their spiral structure. The sample includes both grand design and flocculent spirals (Elmegreen & Elmegreen 1982, 1987) allowing a comparison of the stellar disks in galaxies with different arm morphologies in the optical. Rotation curves based on the axisymmetric decomposition of K maps are compared with the extent of the spiral arms and discussed in terms of the density wave theory.

2. Data

Three optically flocculent or partly multi-armed spiral galaxies (NGC 3223, NGC 5085 and NGC 7085) were observed to allow a detailed study of their spiral structure and a possible decoupling of their stellar and gaseous disks. Two grand design spirals (NGC 5247 and NGC 5861) were also observed to identify differences in stellar disks relating to their optical arm classification. The galaxies are listed in Table 1 with their Hubble type and systemic velocity v_0 from the Revised Shapley-Ames Catalog (RSC) (Sandage & Tammann 1981) while diameters D_{25} and axis ratios R_{25} are taken from the Third Reference Catalog (RC3) (de Vaucouleurs et al. 1991). The linear scales adopted are also given as obtained from the systemic velocity assuming a Hubble constant H_0 = 75 km s^{-1} Mpc^{-1}. All galaxies were classified as ordinary spirals except NGC 5861 which has a weak bar indicated by a SXT5 type in RC3.

The galaxies were observed in the infrared K′-band (Wainscoat & Cowie 1992) and BVI with the 2.2m MPI/ESO telescope at La Silla. The K′ exposures were obtained with the IRAC-2A instrument using the C-lens which gave a pixel size of $0\farcs5$ on the 256×256 NICMOS-3 detector. Mosaics of 2-6 fields were observed for each galaxy depending on their angular size and orientation. Each field consisted of a stack of five 90×2 s exposures. The target fields were interleaved with similar sky exposures taken in different directions approximately 10′ away from the galaxy. This gave a total on-target integration time of 900 s for each field. The individual exposures in a stack were offset by a few arcsec to allow corrections for bad detector pixels. Dome flat-fields were used to correct for the relative sensitivity while the photometric calibration was done using both standard stars and galaxies (NGC 3250, NGC 5090, NGC 6221 and NGC 6744) with known aperture photometry (de Vaucouleurs & Longo 1988). The standard deviation of the transformation of instrument magnitudes to K for both stars and galaxies was 0.08 mag where no color term was used. An average of two nearby sky frames was subtracted from each target exposure before the flat-field correction was done. Stellar images in the sky frames were visually identified and removed by fitting 2D Gaussian profiles which then were subtracted. Objects in the individual frames were used to derive relative offsets within a stack. The average of each stack was computed rejecting outliers (e.g. bad pixels) at a 3σ noise level.

Images in BVI were observed with EFOSC2 which had a pixel scale of $0\farcs33$ on the 1k×1k Thomson THX31156 coated CCD. Sets of 2-3 exposures in each filter were obtained with an exposure time of 600 s in B and 300 s in the other filters except for NGC 5861 for which not B frames were observed. Minor differences between sky and dome flat-fields were corrected by applying a 2D third order polynomial to dome flats which then were used. Photometric calibrations were done using standard stars (Landolt 1992) in the SA110 and MARK-A fields. Significant color terms were found only for B and V filters. Standard deviations of the transformations were $0\fm006$, $0\fm002$ and $0\fm002$ for B, V and I, respectively. The calibration was consistent with the aperture photometry of Longo & de Vaucouleurs (1983). Finally, the average BVI maps were aligned and rebinned to the K′ frames using common stars. The average seeing during the observations was 1″. Foreground stars were removed from the intensity maps by subtracting 2D Gaussian profiles fitted to them.

Spectra of NGC 5085, NGC 5247 and NGC 5861 were taken to estimate their maximum rotational velocity. They were obtained with EFOSC-2 using grism #9 which has a dispersion of 0.11 nm pixel^{-1} at 650 nm. The standard deviation of the wavelength calibration was 0.035 nm derived from the Ar–arc. The spectra were exposed for 600 s with a $1\farcs5$ slit width. Rotation curves were derived from H_α emission lines. The night-sky lines at 630.0 nm, 636.4 nm and 686.4 nm from O I and OH were used as zero velocity reference. Finally, barycentric corrections were applied.

3. Axisymmetric parameters

An accurate determination of sky projection parameters for the galaxies is essential for the study of internal structure such as weak oval distortions and spiral arms. As detailed velocity maps of the galaxies are not available, the two main methods to de-

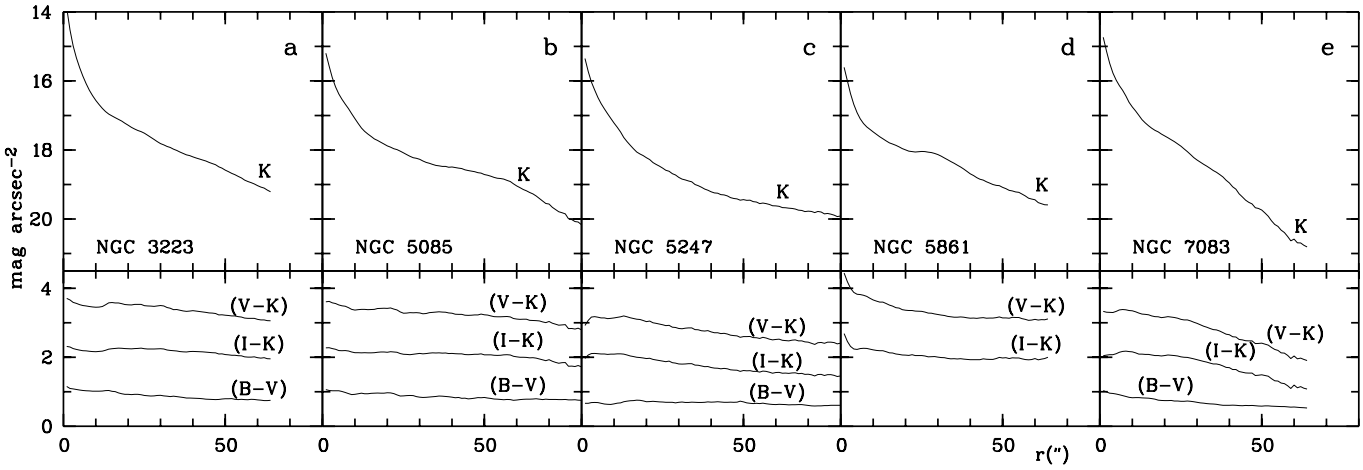

Fig. 1a–e. Mean radial profiles in K and the color indices (V-K), (I-K) and (B-V) for the galaxies.

Table 2. Sky projection parameters for the galaxies. Position (PA) and inclination (IA) angles derived from 2D disk fits and θ_2 phase variations are given together with the radial range used.

	Disk fit			θ_2 phase		
Galaxy	PA	IA	Range	PA	IA	Range
NGC 3223	128°	46°	20-50″	128.°9	44.°9	25-40″
NGC 5085	76°	46°	15-35″	61.°3	48.°5	17-42″
NGC 5247	13°	20°	8-16″	29.°3	26.°6	20-55″
NGC 5861	152°	56°	15-45″	151.°8	55.°0	20-55″
NGC 7083	5°	55°	8-35″	12.°2	50.°4	15-25″

rive the projection are a) fitting a 2D exponential disk to the intensity maps, and b) minimize the radial phase change of the spiral structure across the major axis (Danver 1942). The K′ maps were used for the estimates since they represent the mass distribution in the galaxies better than images in visual bands. The disk fits were done in an annulus in the middle of the exponential disk to avoid influence from either a spherical bulge or possible warps in the outer disks. Even though the effects of spiral structures are reduced by the radial average, open two-armed spirals will bias the results significantly. Such errors were estimated by subdividing the annulus and determining if a systematic radial trend existed. The projection parameters derived are given in Table 2 where also the radial ranges used for the fits are listed.

For all the galaxies, the main two-armed spiral structure in K′ can be traced over a significant azimuthal angle including the position angle found by the disk fitting procedure. The phase θ_2 of the second Fourier component of the azimuthal intensity variation along circles in the plane of the galaxy was computed as function of radius for a grid of projection parameters around the values given in Table 2 for the disk fits. This corresponds to the phase of two-armed spiral pattern for projections close to the true value and is expected to have a smooth radial variation. Small errors in the projection angles will introduce an significant phase change of θ_2 across the major axis while only small effects are seen around the minor axis. The projection parameters were estimated as the values for which the $\theta_2 - \ln(r)$ relation across the major axis showed a minimum deviation from linearity and are listed in Table 2. Significant differences between the two estimates were found for the galaxies NGC 5085 and NGC 5247. They both have open spiral arms for which the exponential disk fits showed a radial dependency. This suggests that the values based on the θ_2-phase are less biased. They were therefore adopted for the sky projection of the galaxies. Typical errors are of the order of 2°.

Radial intensity profiles in K, averaged over circles in the plane of the disks, are presented in Fig. 1a–e where also color indices are given. The standard deviation per pixel of the surface brightness in K′ reaches 0.1 mag at 17.9 mag arcsec^{-2} while it for the visual bands B, V and I first happens at 23.5, 23.0 and 21.5 mag arcsec^{-2}, respectively. The (V-K) color profiles along major and minor axes are shown in Fig. 2. In several cases (e.g. NGC 3223, NCG 5085 and NGC 7083), the (V-K) minor axis profiles display asymmetries around the center suggesting an additional color gradient perpendicular to the major axis. This effect can also be seen on the (V-K) maps of the individual galaxies (see e.g. Fig. 4a–c).

The luminosity profiles in K′ have smooth appearances of Type I (Freeman 1970) suggesting a decomposition into a spherical bulge and an exponential disk. The two fitted components were subtracted from the K′ maps to verify this assumption. Residuals in the outer parts of the galaxies suggest that the exponential scale lengths of the disks were too long. To estimate the effects of young objects in the arm regions, exponential disks were fitted to the K′ intensities in the arm and interarm regions separately. The arm region was defined as the area less than 30° from the mean azimuthal angle of the two-armed spiral pattern. The central intensities and scale lengths for these fits are given in Table 3. The zero point for the K band was taken to 636 Jy (Bessell & Brett 1988).

Three galaxies (NGC 3223, NGC 5085 and NGC 5247) show significant differences between the arm and interarm estimates of the disk scale length. The two remaining galaxies have

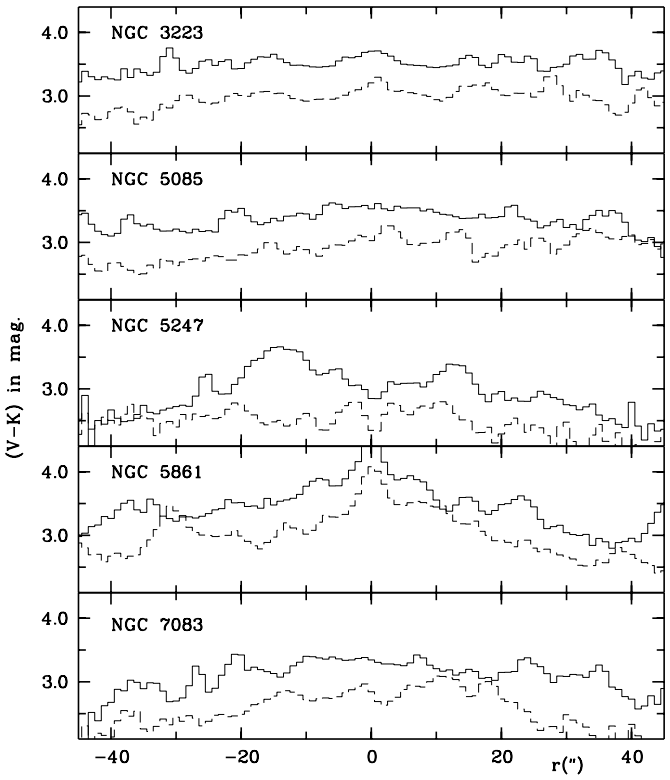

Fig. 2. (V-K) profiles along the major (—) and minor (– –) axes. The minor axis profiles are shifted 0.5 mag down. The radius is given in the plane of the galaxies.

Table 3. Central surface brightness and scale length for exponential disks fitted to the main disk of the galaxies in K′ using either arm or interarm regions. Surface brightness is given in μJy arcsec^{-2}. The average color change in the main disk δ(V-K) per interarm disk scale length is listed with the radial range used.

	Arm		Interarm		Range	δ(V-K)
Galaxy	$\Sigma_{\rm d}$	$h_{\rm d}$	$\Sigma_{\rm d}$	$h_{\rm d}$	($''$)	(mag)
NGC 3223	167	26.″5	215	19.″6	20-35	-0.23
NGC 5085	85	35.″5	81	28.″5	25-35	-0.22
NGC 5247	48	48.″6	70	21.″8	20-60	-0.29
NGC 5861	104	28.″7	90	27.″0	20-50	-0.17
NGC 7083	218	17.″3	172	16.″1	15-35	-0.31

only a marginal steeper interarm disk. They have both slightly asymmetric arms which would decrease the difference based on the average arm location. The many sharp, bright knots and longer scale length in the arm regions measured in K′ suggest an additional contribution of light from young objects in this band. Although the interarm fit will underestimate the central surface brightness slightly, it was adopted as the better representation of the mass distribution of the old stellar disk population. This component was then subtracted from the K′ maps before the inner regions were analyzed.

Significant bisymmetric residuals aligned with the major axis of the galaxies were found in the inner regions after removing the spherical component. This indicates that the central parts also contained a disk component with the same projection parameters as for the outer disk. Two analytical approximations were used to fit the central regions namely a de Vaucouleurs law with variable power $1/n$ plus a flat exponential disk giving the face-on surface brightness:

$$\Sigma(r) = \Sigma_{\rm b} \exp(-(r/h_{\rm b})^{1/n}) + \Sigma_{\rm i} \exp(-r/h_{\rm i}) \quad (1)$$

or a modified Hubble law with an exponent α replacing the bulge part:

$$\Sigma(r) = \Sigma_{\rm b}/(1 + (r/h_{\rm b})^{\alpha}) + \Sigma_{\rm i} \exp(-r/h_{\rm i}) \quad (2)$$

where $\Sigma_{\rm b}$ and $\Sigma_{\rm i}$ denote the central surface brightness for the different components while $h_{\rm b}$ and $h_{\rm i}$ give their scale length. The parameters for the decomposition were estimated by fitting Eq. (1) and Eq. (2) to the 2D surface brightness distribution in K′. Smearing of the central part of the galaxies corresponding to a seeing of $1''$ was included in the fitting procedure. The estimated values of the powers n and α are noted in Table 4 but are rather uncertain due to seeing effects and possible sensitivity variation within individual pixels. For the final decomposition, a modified Hubble law (i.e. $\alpha = 2$) was adopted because its goodness of fit was similar to that of the other models and its analytical form was simpler. The parameters for the components adopted are given in Table 4.

Accurate rotation curves for the galaxies are required for a dynamic interpretation of the spiral structure. Most rotation curves are obtained from emission line spectra and refer to gas kinematics rather than to motion of the stellar disk. Further, the detailed shape of the inner rotation curve (i.e. the angular velocity Ω) is not accurately determined due to its steep gradient and seeing effects. These problems make it impossible to derive a reliable estimate of the epicyclic frequency $\kappa(r) = 2\Omega\sqrt{1 + 1/2\,(d\ln\Omega/d\ln r)}$ directly from the measured velocities in the inner region where the Inner Lindblad Resonance (ILR) is expected. An alternative approach is to estimate the rotation curve from the mass distribution obtained through the K′ surface brightness maps assuming a constant mass-to-light ratio and a geometry for the components (see e.g. Kent 1986). The galaxies were assumed to have four components, namely: a) a spherical bulge, b) two flat exponential disks, and c) a spherical halo. The mass distribution of the bulge component was derived assuming the modified Hubble profile Eq.(2) with $\alpha = 2$ while the halo was modeled by a logarithmic potential. The circular velocity $v_{\rm c}$ at radius r is then given by (ref. Binney & Tremaine 1987; Abramowitz & Stegun 1965):

$$\begin{aligned} v_{\rm c}^2(r) \;=\; & 2\pi {\rm G}\sigma_{\rm b}\frac{h_{\rm b}^2}{r}({\rm F}(\varphi \setminus \pi/2) - {\rm E}(\varphi \setminus \pi/2)) + \\ & 4\pi {\rm G}\sigma_{\rm i} h_{\rm i} y_{\rm i}^2({\rm I}_0(y_{\rm i}){\rm K}_0(y_{\rm i}) - {\rm I}_1(y_{\rm i}){\rm K}_1(y_{\rm i})) + \\ & 4\pi {\rm G}\sigma_{\rm d} h_{\rm d} y_{\rm d}^2({\rm I}_0(y_{\rm d}){\rm K}_0(y_{\rm d}) - {\rm I}_1(y_{\rm d}){\rm K}_1(y_{\rm d})) + \\ & \frac{v_{\rm H}^2 r^2}{h_{\rm H}^2 + r^2} \end{aligned} \quad (3)$$

where ${\rm I}_0, {\rm K}_0, {\rm I}_1, {\rm K}_1$ are modified Bessel functions with the argument $y_{\rm i,d} = r/(2h_{\rm i,d})$ and $\varphi = \sqrt{r^2/(h_{\rm b}^2 + r^2)}$ is the amplitude of the incomplete elliptic integrals E and F. The halo

Table 4. Parameters for the decomposition of the K′ maps into a spherical bulge and two flat disk components including maximum velocity and scale length for the halo adopted. The best estimate of the powers n and α for a free bulge fit are listed. The barycentric systemic velocity v_0 and maximum rotational velocity $v_{\rm m}$ in the plane of the galaxy obtained from the long slit spectra are given together with the position angles used for the observations. Surface brightness is in mJy arcsec^{-2}, velocity is in km s^{-1}, and M/L ratio is in solar units.

	Bulge		Inner disk		Main disk		Halo		Bulge					
Galaxy	$\Sigma_{\rm b}$	$h_{\rm b}$	$\Sigma_{\rm i}$	$h_{\rm i}$	$\Sigma_{\rm d}$	$h_{\rm d}$	$v_{\rm H}$	$h_{\rm H}$	n	α	PA	v_0	$v_{\rm m}$	M/L
NGC 3223	4.876	0.″33	1.397	2.″18	0.215	19.″6	251	70″	1.5	1.7	-	-	-	0.8
NGC 5085	0.442	1.″59	0.153	4.″66	0.081	28.″5	141	58″	1.8	1.9	24°,90°	1940	141	0.6
NGC 5247	0.400	0.″96	0.268	4.″76	0.070	21.″8	149	47″	4.1	4.4	14°,90°	1354	-	0.7
NGC 5861	0.085	1.″71	0.482	1.″51	0.090	27.″0	158	64″	2.6	1.6	149°	1843	158	0.7
NGC 7083	0.863	0.″95	0.288	4.″24	0.172	16.″1	223	73″	3.7	1.3	-	-	-	0.7

component is defined by its maximum circular velocity $v_{\rm H}$ and scale length $h_{\rm H}$ while G is the gravitational constant. The surface densities $\sigma_{\rm b,i,d}$ for the bulge and disk components were assumed to be proportional to the central K′ surface brightnesses $\Sigma_{\rm b,i,d}$ after the geometric projection correction was applied to the flat disk components. The scale length derived from the decomposition was used for the different components.

The rotation curve Eq. (3) was fitted to observational data obtained from the long slit spectra and from Rubin et al. (1982) for NGC 3223 and NGC 7083. All radial velocities were corrected for projection effect assuming plane circular motions in the galactic disks. The halo velocity $v_{\rm H}$ was taken to be equal to the maximum rotational velocity of the galaxy at large radii. The optical determination agreed with the H I W_{20} line width data (Fisher & Tully 1981; Aaronson et al. 1982) except for NGC 5861 which displays a slight asymmetry in its outer part. The remaining two parameters, mass-to-light ratio M/L and halo scale length, were obtained from the fit to the rotation curves for NGC 3223 and NGC 7083 while the uncertainties of the kinematic data for the remaining galaxies only allowed the maximum rotational velocity $v_{\rm m}$ to be determined. In these cases, M/L and $h_{\rm H}$ were derived assuming the maximum rotational velocity of the disk was equal to 63% of the total circular velocity of the galaxy (Bottema 1997). The parameters for the rotations curves are given in Table 4 where also the M/L ratio in solar units is given.The rotation curve for NGC 3223 is shown in Fig. 3a and b, as an example, together with its angular velocity $\Omega(r)$ and curves for $(\Omega-\kappa/2)$, $(\Omega-\kappa/4)$ and $(\Omega+\kappa/2)$.

A thick exponential disk with a radial to vertical scale length ratio of 5:1 would yield a 3% larger M/L value. This does not change the shape of the rotation curve significantly. A higher fraction of young object in the main disk compared to the bulge region would give a much larger effect. Population synthesis models of spiral galaxies (Chiosi & Vallenari 1996) estimate that 20-25% of the light in the K-band may come from young stars assuming a constant star formation rate. To estimate this effect, rotation curves for models with a M/L for the main disk reduced to 0.7 of the value for the bulge were computed (see Fig. 3b). The general behavior remains the same whereas small changes in the bulge region can be seen due to the increase of its mass.

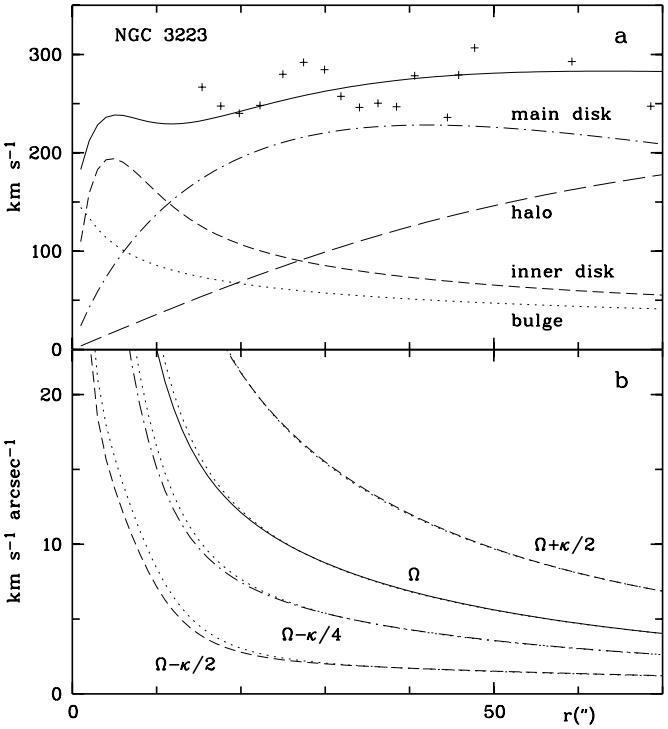

Fig. 3a and b. Rotation and angular velocity curves as function of radius for NGC 3223: **a** total rotation velocity curve including curves for individual components and velocity points observed, **b** angular velocities Ω, $(\Omega-\kappa/2)$, $(\Omega-\kappa/4)$ and $(\Omega+\kappa/2)$. The dotted curves show a model where the M/L for the main disk was reduced to 0.7 of the bulge value.

4. Morphology and spiral structure

Several corrections were applied to the K′ maps before the shape and amplitude of the spiral patterns could be estimated and analyzed. The spherical bulge component was subtracted from the intensity maps prior to the de-projection. Further, a correction for population effects must be included since star formation in the arms will introduce significant systematic errors. Although the K′ images have a much smoother appearance than bluer images, there are many well defined knots along the spiral arms. Diffusion of stellar orbits would dissolve knots consisting of

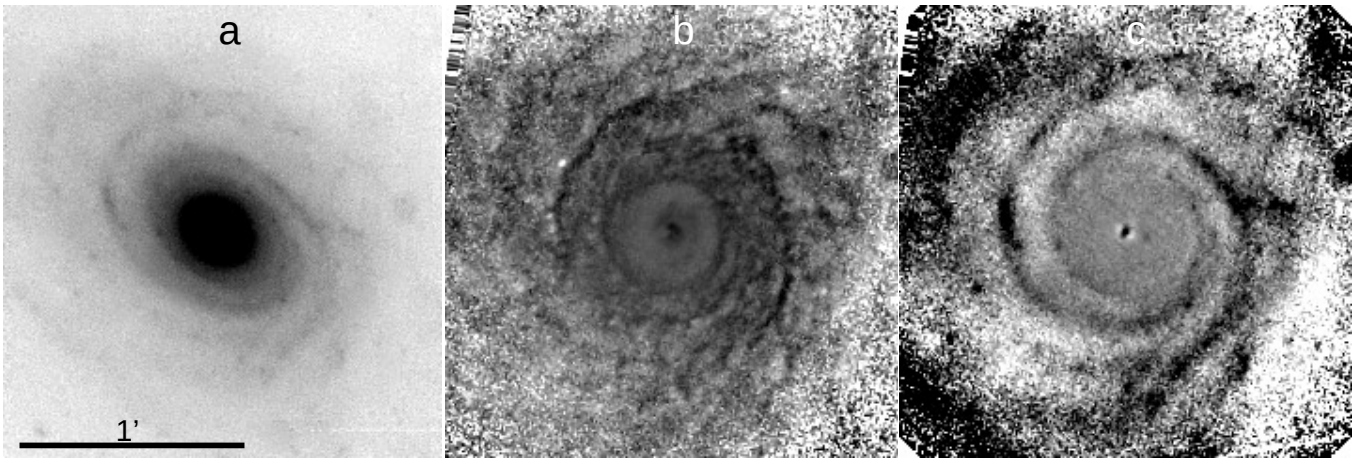

Fig. 4a–c. Surface brightness maps of NGC 3223: **a** K′ intensity map, **b** de-projected (V-K′) color map, **c** de-projected map of the K′ intensity relative to the axisymmetric background and with the bulge component subtracted. Foreground stars were removed. Higher intensities and redder colors are presented darker in the figure. The bar corresponds to 1′ on the sky.

stars in less than 50 Ma (Wielen 1977). The concentration of knots in the arm regions suggest that they are younger than the typical time – less than 40 Ma – which it takes the density wave to pass the given location. This indicates that the knots are associated with very young objects and that a significant fraction of the K′ light in the arm regions originates from Population I objects. The fraction is expected to be larger in the arms where star formation is higher and emission from H II regions may be important.

It is very difficult to disentangle population effects from attenuation due to dust (Witt et al. 1992) especially since they are spatially correlated. Further, ages for stellar populations older than 2-3 Ga cannot be reliably determined from their (V-K) colors (Charlot et al. 1996). The strong dust lanes along the arms, seen on B images, can hardly be traced on the K′ frames which indicates that dust effects are not important in this band. Without spectroscopic information, it is not possible to deduce the population composition in the arm regions including the knots and thereby derive a reliable correction across arms.

To reduce such population effects, it was assumed that a major part of the luminosity from sharp knots originated from Population I objects and that this contribution therefore should be significantly reduced in the analysis of the old stellar disk. This was done by computing a residual map between the actual K′ image and the one represented by the 8 lowest Fourier components of the azimuthal intensity variations. All intensities larger that 5σ in this map were subtracted from the original K′ frame. This removed all major knots but retained sharp features in the central regions of the galaxies. The radial amplitude and phase variation of the spiral patterns were then derived from the Fourier components of azimuthal intensities of these cleaned K′ maps. This procedure reduced the influence of knots but does not correct for the continuous contribution of young objects in spiral arms. The behavior of the individual galaxies are described in the following sections.

4.1. NGC 3223

The galaxy is classified as a Sb(s)I-II in RSC while RC3 assigns the type SAS5 with luminosity class 2.3. The K′ and (V-K′) maps are given in Fig. 4a–c where also the relative amplitude of non-axisymmetric features is shown. NGC 3223 has a multi-arm, flocculent appearance on B images whereas the K′ map shows a symmetric, two-armed spiral. Interpreting the color variations on the (V-K′) map as mainly due to attenuation by dust, the flocculent spiral structure in blue colors is less related to the mass perturbations in the old stellar disk than to the distribution of dust and gas in the disk.

The K′ luminosity profile (Fig. 1a) is well fitted with an exponential disk outside a radius of 20″ whereas the inner part is best approximated by a combination of an inner exponential disk and a spherical bulge. The aspect ratio of the inner disk is marginally smaller than that of the outer disk which could suggest it being thicker. The (V-K′) color has a local maximum around 15″ where a dust ring with (V-K′)$\approx 3\overset{\mathrm{m}}{.}7$ is seen (Fig. 4b). Inside this radius the color map shows little structure except for a weak one armed spiral feature in the very center. Further, a general color gradient perpendicular to the major axis is noted.

The radial variation of the amplitude a_2 and phase θ_2 of the two-armed spiral (Fig. 5b,c) show not significant oval distortion in the central region (i.e. $a_2 < 2\%$). The main two-armed spiral pattern starts at $r = 20''$ just outside the dust ring and can be traced to a radius of almost 40″ on the relative intensity K′ map (Fig. 4c) where interarm features appear and a small phase shift can be seen. The amplitude a_4 of the m=4 component is lower than a_2 in the region of the main symmetric spiral out to $\approx 38''$ where it becomes relative more important. The ratio a_4/a_2 shows a maximum at 42″ while it is of order unity in the outer parts.

The dust ring and the start of the main spiral pattern just outside suggest that a major resonance (i.e. ILR or corotation (CR)) is located in the radial region $15'' \leq r < 20''$ while the end of the symmetric two-armed spiral and the maximum

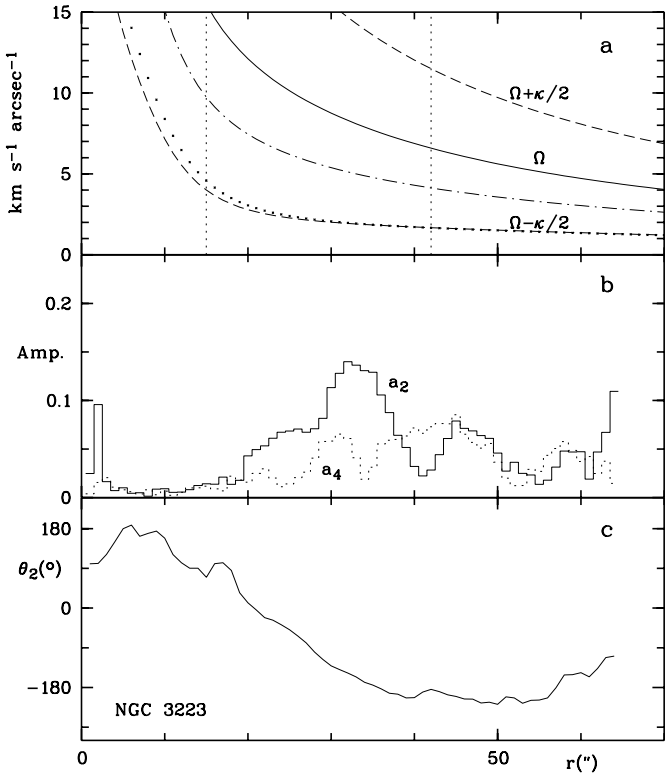

Fig. 5a–c. Angular velocity curves, and amplitudes and phase of the spiral pattern for NGC 3223 as function of radius: **a** angular speeds Ω, (Ω-κ/2), (Ω-κ/4) and (Ω+κ/2), **b** relative amplitudes a_2 and a_4, **c** phase θ_2. The vertical lines indicate likely locations of major resonances (see text). The dotted (Ω-κ/2) curve shows a model with a M/L of the main disk reduced to 0.7 of the bulge value.

of the a_4/a_2 ratio indicate another resonance (e.g. 4:1, CR or Outer Lindblad Resonance (OLR)) around 42″. Assuming a single pattern with constant angular speed $\Omega_{\rm p}$, only one value of $\Omega_{\rm p}$ places resonances at the radii suggested above (Fig. 5a) namely $\Omega_{\rm p}$ = 26.0 km s^{-1} kpc^{-1} with the main spiral located between ILR and 4:1. The strong, symmetric spiral breaks up into a weak multi-armed pattern around 42″ in agreement with dynamic models of the 4:1 resonance region (Contopoulos & Grosbøl 1988; Patsis et al. 1991, 1997).

4.2. NGC 5085

NGC 5085 is also classified as a SAS5 galaxy in RC3 and has an arm class of 2 specifying fragmented spiral arms with no regular pattern (Elmegreen & Elmegreen 1982). Contrary to this description, the K′ image (Fig. 6a) shows an open, grand design spiral structure. The strong spiral pattern makes it difficult to determine the sky projection parameters directly from 2D fit of an exponential disk to its K′ image. The orientation of the major axis estimated from the θ_2 phase variation and that derived from the two long-slit spectra, assuming circular velocities, agree within 2° but differ by more than 20° from the value given in RC3. This also affects the estimated inclination angle which is significantly higher than that suggested by the RC3 value for R_{25}.

The spiral structure on the B image appears to reach much closer to the center than the K′ spiral. This impression is created by the very sharp dust lanes as seen on the (V-K′) map (Fig. 6b) which penetrate to an inner radius of 4″ while the spiral pattern in K′ only can be traced in to a radius of 13″. Outside this radius, the main dust lanes are located on the inner side of the spiral arms. The axisymmetric K′ profile (Fig. 1b) suggest a shorter scale length of the disk outside 60″. This may rather be due to an excess of light from young objects in the main spiral arms inside this radius than to change in the old stellar disk population. The colors show a smooth radial variation without significant features. The (V-K′) map suggests a weak color gradient perpendicular to the major axis.

The radial variation of θ_2 (Fig. 7c) shows the main two-armed spiral starting around 14″ and reaching almost 45″ where the phase gets constant possibly caused by a warp, a small projection error, or a minor residual in the sky background. In the inner regions an oval distortion with an amplitude of $a_2 \approx 0.1$ can be identified in the radial range 7-13″ while a tight inner spiral is visible inside 5″ with $a_2 < 0.1$. The main spiral has an amplitude around 0.1 in the inner parts but increases to almost 0.2 at a radius of 30″. The a_4 amplitude increases at the start of the main spiral and becomes equal to a_2 at 42″. The absolute amplitude of the spiral pattern is not significant compared to the uncertainty of the average K′ intensity outside 50″. At this radius, small errors in the projection become important causing the steep increase in a_2.

The transition between the oval distortion and the main two-armed spiral occurs in the region 10-15″ and suggests a major resonance in this radial range. Similarly, the peak of the a_4/a_2 ratio at 42″ and the end of the symmetric spiral pattern just outside this radius indicate another resonance. The only pattern speed $\Omega_{\rm p}$ which locates major resonances close to these radii is 18.9 km s^{-1} kpc^{-1}with ILR at 12″ and 4:1 at 41″. The CR would be at a radius of $\approx$ 77″ which roughly corresponds to the outer limit of the spiral structure seen on the B image.

4.3. NGC 5247

It is a grand design spiral galaxy with arm class 8 and classified as SAS4 in RC3. The very strong arms in K′ make the determination of its sky projection difficult. The parameters derived from the θ_2 phase variation agrees reasonably well with both the value given in RC3 and the one derived from the two long slit spectra considering that NGC 5247 is nearly face-on.

The axisymmetric K′ luminosity profile (Fig. 1c) shows a very slow transition between the inner bulge region and an outer exponential disk. The large difference between the arm and interarm estimates of the disk scale length suggests that the outer part of the K′ profile is dominated by the contribution from the spiral arms. The (V-K′) color is almost constant at $3\overset{\rm m}{.}2$ in the range 3-14″ while it decreases slowly outside this region. The color map (Fig. 8a–cb) shows a complex structure inside 18″ possible due to an inner dust spiral.

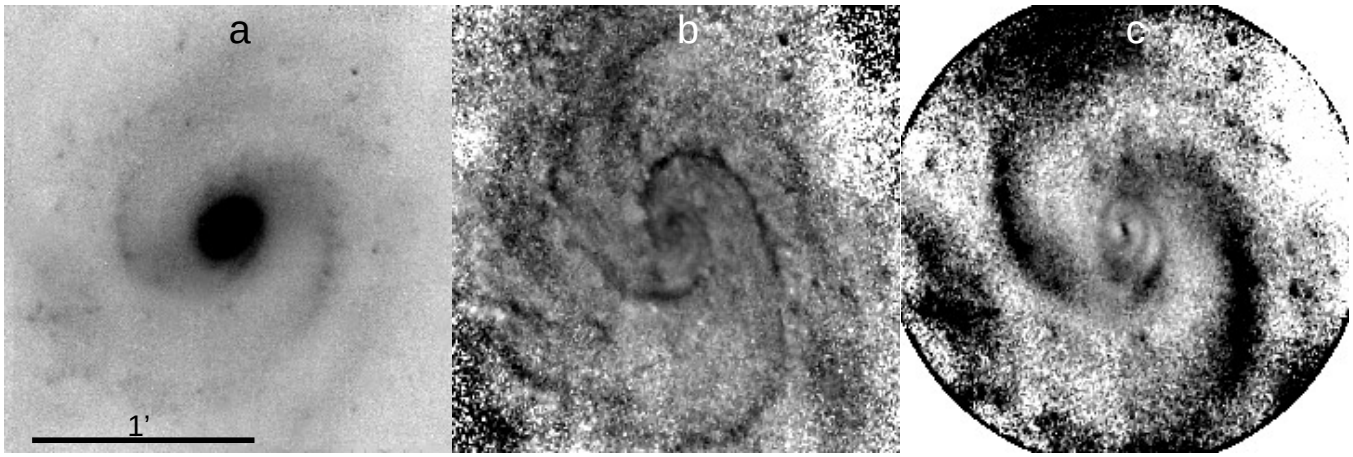

Fig. 6a–c. K′ surface brightness (**a**), (V-K′) color (**b**) and relative K′ intensity maps (**c**) for NGC 5085 as in Fig. 4a–c.

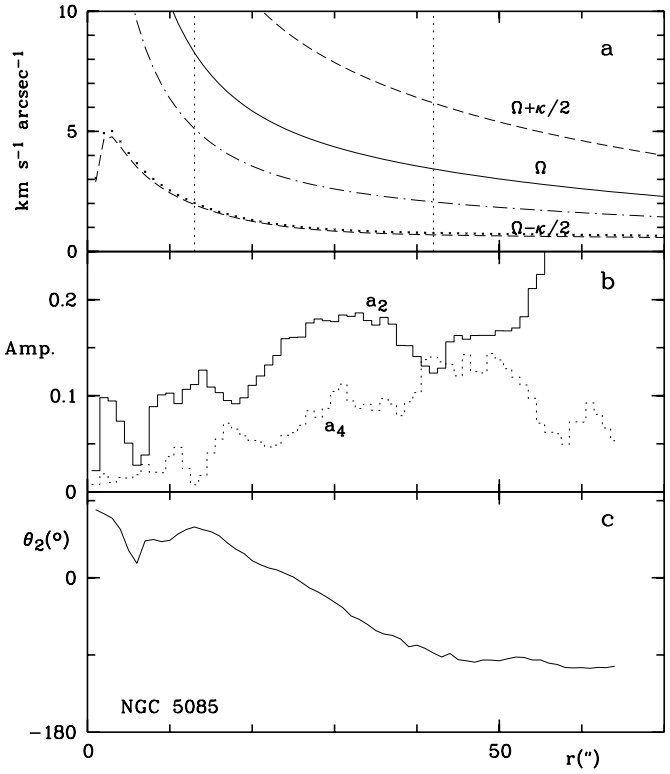

Fig. 7a–c. Angular velocity curves (**a**), amplitudes $a_{2,4}$ (**b**) and phase θ_2 (**c**) of the spiral pattern in NGC 5085 as in Fig. 5a–c.

The spiral pattern can be traced in to a distance of $2''$ on the B image while the main two-armed spiral on the K′ map first starts around $19''$ (Fig. 8a–cc). This is due to inner dust lanes as in the case of NGC 5085. A sharp one-armed spiral feature is also seen in the inner region. Its sharpness suggests it to be associated with Population I objects rather than with a density enhancement in the inner disk. A very blue lane with (V-K′) $\approx 2\overset{\mathrm{m}}{.}7$ is located along the one-armed structure.

The radial variation of θ_2 given in Fig. 9c shows an oval distortion with $a_2 = 0.05$ for $6'' < r < 15''$. Inside this region, θ_2 is close to 0° which may be caused by a small error in the fit of the central disk and bulge components due to the oval distortion. The main two-armed spiral starts around $19''$ and can be traced to the edge of the K′ image close to a radius of $90''$. The spiral changes pitch angle around $r = 44''$ where it becomes more open and again at $63''$ where the pattern starts to be tighter than its inner part. The amplitude of the spiral cannot be estimated reliably in the outer parts of the galaxy (i.e. $30'' < r$) due to the low K′ surface brightness in the interarm regions. This makes the values of a_2 and a_4 approach unity at large radii.

The small inclination angle makes the rotation curve unreliable due to the large projection correction. Considering the uncertainties, the maximum rotational velocity estimated from the long slit spectra is compatible with the W_{20} value by Fisher & Tully (1981). The latter was used to model the rotation curve. Due to the lack of a accurate rotation curve, it was assumed that the maximum rotational velocity of the outer disk was 63% of the total rotational speed (Bottema 1997).

The start of the main spiral pattern at $19''$ suggests that the ILR is located just inside this radius. This gives Ω_{p} = 20.3 km s^{-1} kpc^{-1}and places 4:1 around $68''$. The main spiral becomes tighter and the arms bifurcate close to this radius as expected at the 4:1 resonance.

The current rotation curve for NGC 5247 differs from the one used by Contopoulos & Grosbøl (1986,1988) in several aspects. Besides differences due to the adopted distance and sky projection, the form defined by Eq. 3 is more directly based on a mass model. This shifts the location of the resonances but does not alter the general dynamic behavior.

4.4. NGC 5861

The classification SXT5 in RC3 indicates the presence of a weak bar while its grand design spiral pattern has an arm class 12. The two-armed spiral is also very prominent in K′ outside $r = 12''$ as seen in Fig. 10a. The (V-K′) map (Fig. 10b) shows a filamentary structure in the region of the main spiral with many interarm dust spurs. The color gets increasingly red towards the center with

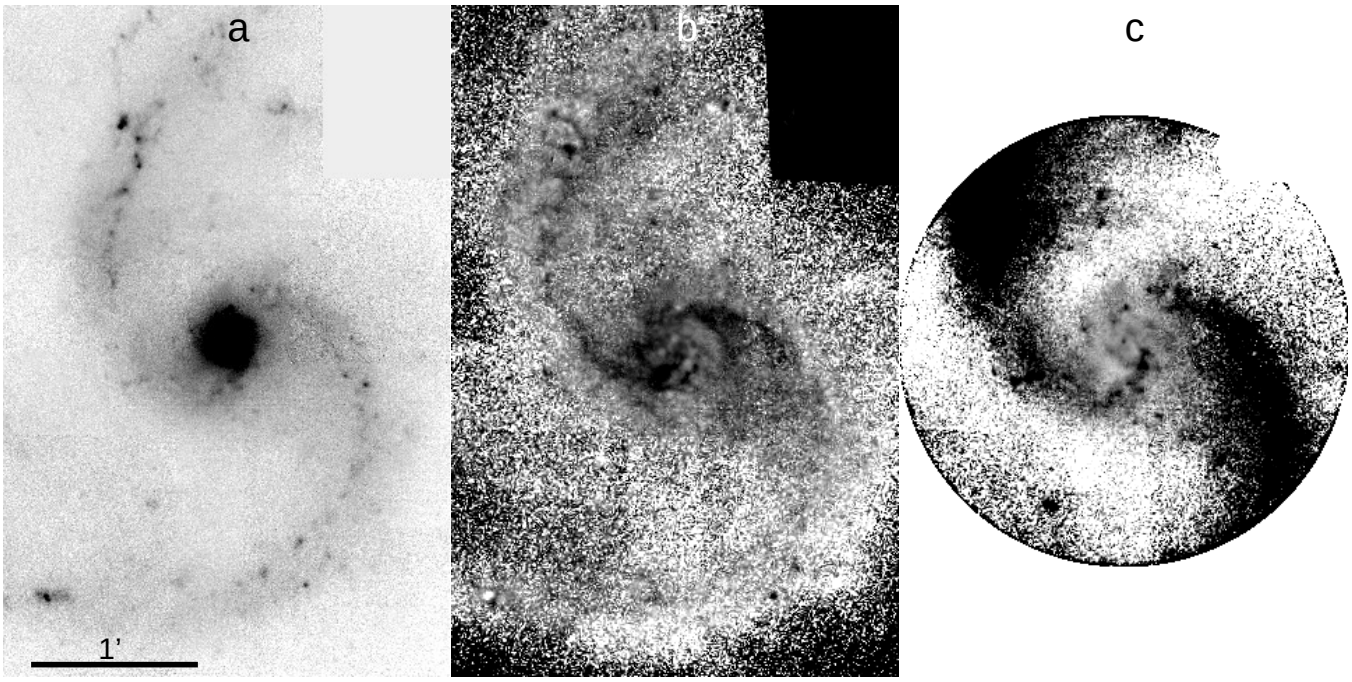

Fig. 8a–c. K′ surface brightness (**a**), (V-K′) color (**b**) and relative K′ intensity maps (**c**) for NGC 5247 as in Fig. 4a–c.

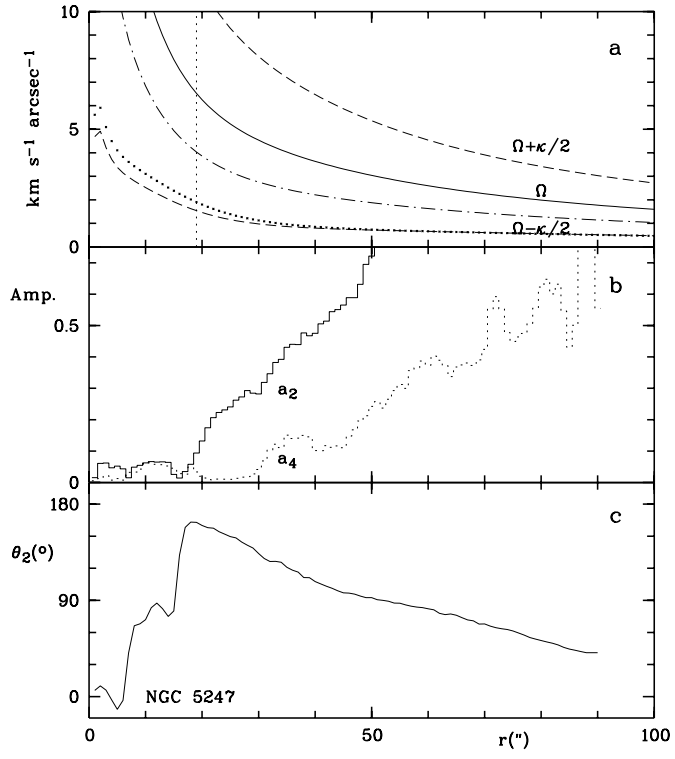

Fig. 9a–c. Angular velocity curves (**a**), amplitudes $a_{2,4}$ (**b**) and phase θ_2 (**c**) of the spiral pattern in NGC 5247 as in Fig. 5a–c.

(V-K′) $> 3^{\rm m}.7$ around the start of the spiral. Patches of spiral dust lanes continue inside the stellar spiral. The many knots and sharp ridges along the spiral arms seen on the relative K′ intensity map (Fig. 10c) suggest a significant contribution of light from young objects in the arm regions.

The K′ profile given in Fig. 1d shows a very steep bulge region and an exponential disk outside a radius of $10''$ with an intensity excess in the interval 25–$40''$ which corresponds to the region where the sharp features are seen in the arms. The average color changes very slowly in the outer parts of the disk. A weak color gradient perpendicular to the major axis can also be observed in this galaxy.

The θ_2 phase is almost constant at 100° inside a radius of $10''$ (Fig. 11c). This oval distortion has an amplitude of $a_2 \approx 0.07$. The two-armed spiral starts around $12''$ and reaches an amplitude of 14% inside $25''$ whereas the peak of more than 20% at $32''$ may be due to Population I objects seen on the K′ map. Close to $40''$ the a_4/a_2 ratio increases significantly with a peak at $43''$. Further, the main spiral breaks up into several branches just outside this radius. The increase of a_2 outside this radius is mainly due to the low interarm intensities. The θ_2 phase shows small jumps of $\approx 7^\circ$ around $44''$ and $53''$ while the pitch angle of the two-armed pattern remains almost constant.

The maximum rotational velocity of 158 km s^{-1} obtained from the long slit spectrum does not fully agree with the value from HI W_{20} line width data (Fisher & Tully 1981). The asymmetry and patches in the outer parts of NGC 5861 on visual images could suggest a disturbed velocity field in this region. Thus, the optical data were used to estimate the maximum rotational speed of the galaxy. The rotation curve shows a very steep raise in the central part. This cannot be reproduced by a model based on a common M/L ratio for both bulge region and outer disk. A satisfactory fit was achieved for a M/L ratio of the outer disk reduced to 0.4 of the value for the bulge components.

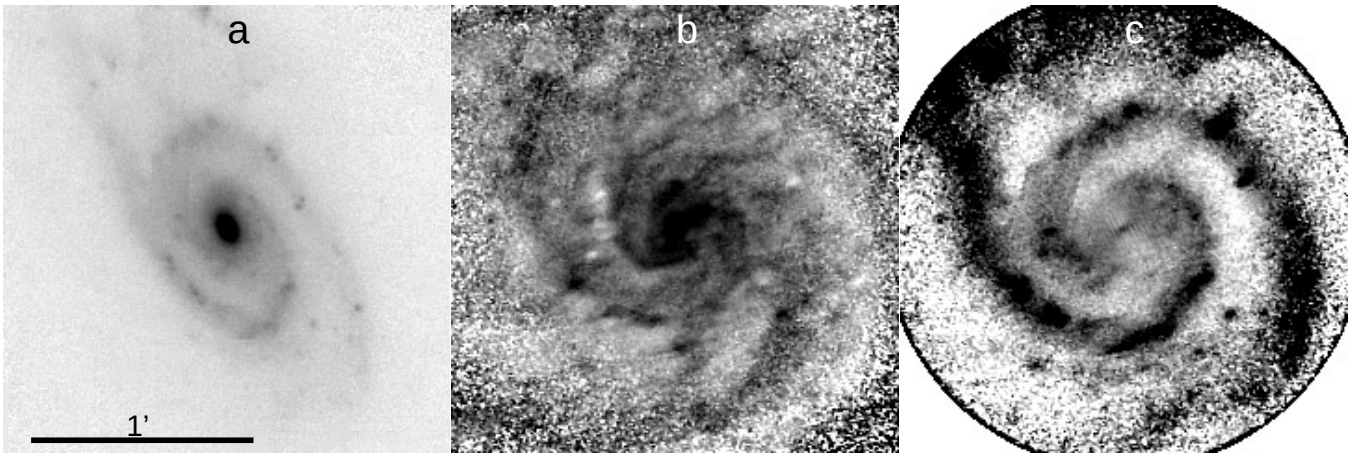

Fig. 10a–c. K′ surface brightness (**a**), (V-K′) color (**b**) and relative K′ intensity maps (**c**) for NGC 5861 as in Fig. 4a–c.

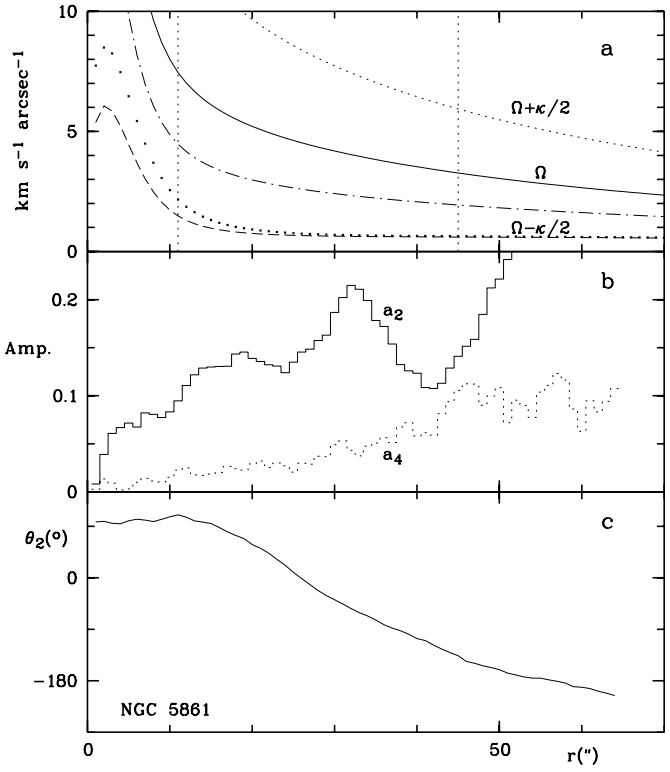

Fig. 11a–c. Angular velocity curves (**a**), amplitudes $a_{2,4}$ (**b**) and phase θ_2 (**c**) of the spiral pattern in NGC 5861 as in Fig. 5a–c. The dotted (Ω-κ/2) curve represents a model with a M/L for the outer disk reduced to 0.4 of the value of the bulge.

The model is shown as the dotted curve on Fig. 11a. The relative small bulge of this galaxy reduces the effects.

The end of the oval distortion at $10''$ and the strong two-armed spiral starting just beyond $12''$ indicate a major resonance in this radial interval. The increase of the a_4/a_2 ratio together with the termination of the strong spiral on the visual maps around $45''$ make the location of another resonance at this radius likely. From the angular velocity curve in Fig. 11a, the best value for the pattern speed which places major resonances close to these two radii is 17.9 km s^{-1} kpc^{-1}. With this value, the resonances ILR, 4:1 and CR are located at $9''$, $43''$ and $84''$, respectively. The model with reduced M/L for the outer disk would have ILR at $11''$ while the other resonances would retain their locations. If CR would be placed close to $45''$, the ILR would be at $6''$ which is inside the oval distortion and therefore less likely.

4.5. NGC 7083

The galaxy is the most distant in the sample and has the morphological type SAS4 in RC3 with a multiple arm appearance on the B image. The K′ maps (Fig. 12a,c) show a grand design two-armed spiral. A double arm structure at the end of the strong symmetric arms is observed. This is very similar to features seen in models (Patsis et al. 1997). The main spiral does not fully cross the major axis which makes the determination of sky projection parameters more uncertain. Thus, the best θ_2 phase determination close to the dynamical major axis of PA = 11° (Rubin et al. 1982) was adopted. The (V-K′) color map (Fig. 12b) shows strong dust lanes along the inner side of the main spiral pattern but also significant dust patches in the interarm regions. A color gradient perpendicular to the major axis can be seen clearly.

The axisymmetric K′ profile (Fig. 1d) has a smooth disk component with a very short scale length. Also the radial color variation in (V-K′) and (I-K′) is larger than for the other galaxies. The color gradient seems to steepen at a radius around $25''$ where the strong two-armed pattern terminates. The (B-V) color shows a much smaller radial change.

The a_2 amplitude and θ_2 phase diagrams given in Fig. 13b,c suggest a weak open spiral inside $5''$ with $a_2 \approx 0.03$. This inner spiral goes into an oval ring structure between 9-$11''$ which has a relative amplitude of 0.04. The main two-armed spiral starts just outside this radius with $a_2 = 0.13$ in the interval $12'' < r < 20''$. Its amplitude peaks around $27''$ with a values close to 0.4 after which it decreases. The signal-to-noise ratio is not high enough to trace the spiral outside $37''$ where a_2

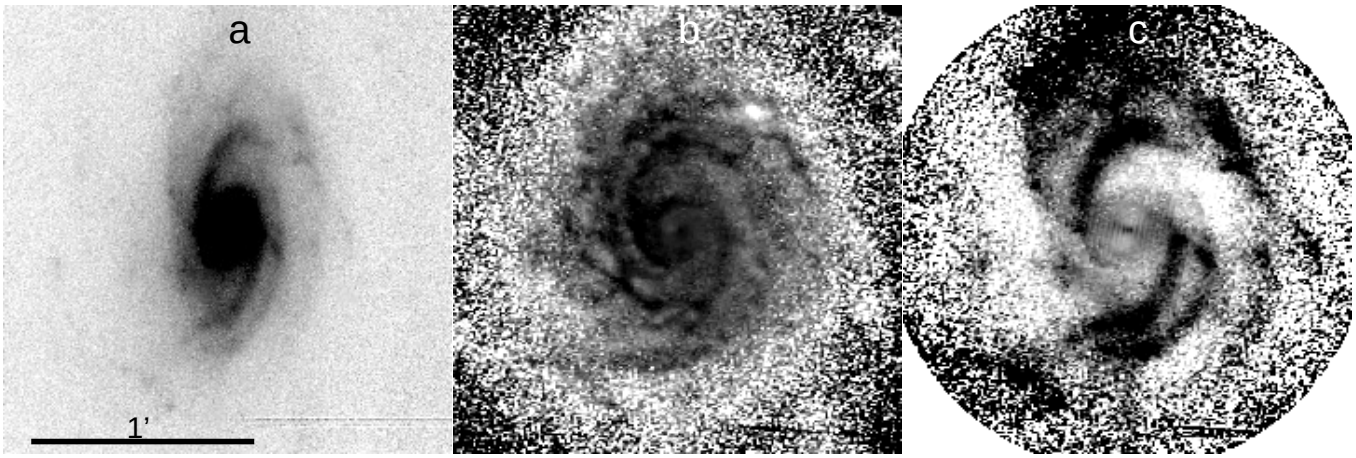

Fig. 12a–c. K′ surface brightness (**a**), (V-K′) color (**b**) and relative K′ intensity maps (**c**) for NGC 7083 as in Fig. 4a–c.

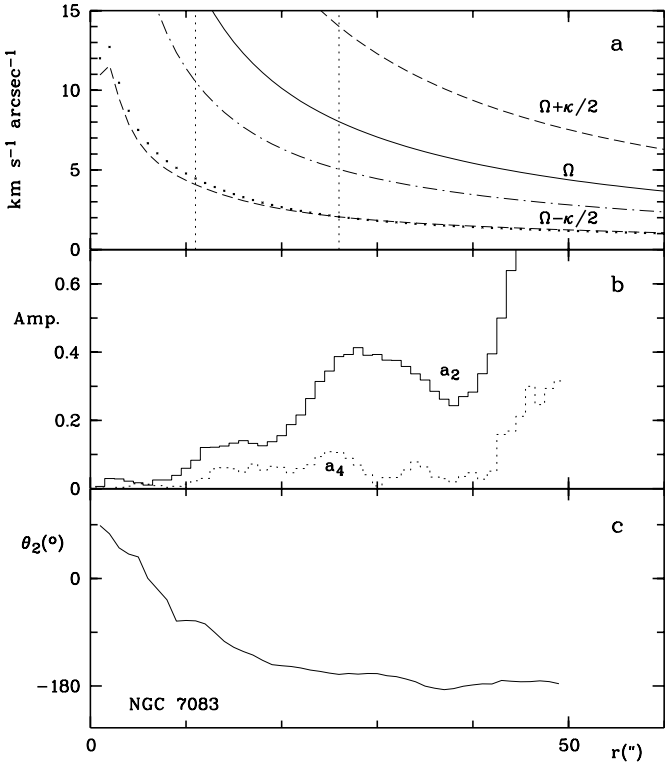

Fig. 13a–c. Angular velocity curves (**a**), amplitudes $a_{2,4}$ (**b**) and phase θ_2 (**c**) of the spiral pattern in NGC 7083 (see Fig. 5a–c).

starts to increase and the θ_2 phase becomes almost constant. The radial θ_2 variation suggests that the main spiral spans the region 12-26″ since θ_2 is almost constant just outside this range. The amplitude a_4 has a local maximum at 25″ which could be associated to the end of the strong symmetric two-armed pattern (see Fig. 12c).

It is likely that ILR or CR is located around 11″ where the ring structure and inner limit of the main spiral are placed. Further, the end of the two-armed pattern and local maximum of a_4 suggest another resonance close to 26″. A pattern speed of 26.2 km s^{-1} kpc^{-1}is the only solution which places major resonances near these two radii namely ILR and 4:1. This value of $\Omega_{\rm p}$ locates CR at $44''$ which corresponds to the outer limit for strong arm filaments seen on the B image. Weaker arm fragments can be traced to almost 75″ where OLR would be located.

5. Discussion

All five galaxies show clear two-armed, grand design spiral structure in their disks as seen in K′ although three of them would be classified as flocculent on blue images. This strongly suggests that the arm classification by Elmegreen & Elmegreen (1982) relates more to the properties of dust and gas in the disk than to the underlying density perturbation in the stellar disk. The Population II disks in the three optically flocculent galaxies do not display any significant difference compared to those of the grand design spirals in the sample. This supports the view that stellar and gaseous disks are decoupled in optically flocculent spirals (Block et al. 1994). The morphology of their old stellar disks covers a significant range as discussed by Block (1996) including galaxies with prominent spiral density perturbations (e.g. NGC 3223), with very weak density arms as in NGC 2841 (Block et al. 1996) or with multi-arm structures (e.g. NGC 2976).

A standard decomposition of the K′ maps into two axisymmetric components (i.e. a spherical bulge and a flat exponential disk) was not satisfactory for any of the five galaxies. Significant bisymmetric residuals, aligned with the major axis, were found in the central regions. These residuals can be removed by including a central exponential disk component with project parameters equal to those of the main disk. This is consistent with de Jong (1996) and Courteau et al. (1996) who found that exponential bulge are common in late-type disk galaxies. The steep inner disks are similar to the nuclear disk found in E-S0 galaxies (van der Bosch et al. 1994; Scorza & Bender 1995; Seifert & Scorza 1996). There is weak evidence from the fit of the inner disk in NGC 3223 that it has a smaller aspect ratio than the outer disk and therefore may be marginal thicker. Oval distortions seen in several of the galaxies make it very difficult to estimate reliable aspect ratios. After subtracting all three com-

ponents from the K′ maps, a small point like residual remained in the center. This may be an artifact due to pixel level errors in the stacking and non-uniform sensitivity of individual pixels.

The mass-to-light ratio of the luminous matter in K′ is around 0.7 in solar units which is compatible with values by Héraudeu et al. (1996) but somewhat lower that those found by e.g. Quillen (1996). If a maximum disk solution had be chosen for the decomposition, the M/L would increase and be in the range 0.8-1.3. The shape of the inner rotation curve and therefore the location of resonances would not be changed significantly.

Three galaxies (NGC 3223,NGC 5085 and NGC 7083) display a significant color gradient perpendicular to their major axes with Δ(V-K′) $\approx 0\overset{\mathrm{m}}{.}2$. This alignment makes it appear as a projection effect due to dust. Brightness gradients due to dust are discussed by Byun et al. (1994). A detailed discussion of (V-K) color gradients across the minor axis of spirals, including dust, are to appear in a forthcoming paper by Elmegreen and Block (1998) who demonstrate that exponential disks can produce marked asymmetries. A systematic offset of thick dust lanes relative to young objects in the spiral arms would give additional asymmetries in the (V-K) color maps as seen in NGC 5085 (Fig. 6b), where the dust lanes appear to be more pronounced on one side of the minor axis compared to the other.

The main two-armed spiral can be fitted with a logarithmic spiral over a significant radial interval as seen in Fig. 14. The absolute value of the pitch angle $|i_2|$ or the radial wavelength increases in the inner part of the pattern i.e. just outside the region where the oval distortions terminate. The increasing wavelength could partly be caused by interference with the weak bar component. The amplitude of the oval distortions is, in all cases, smaller than that of the main spiral pattern. Furthermore, a phase shift between the end of the oval and the start of the spiral is observed in several cases. These points support the increase of the radial wavelength in the inner part of the spiral as being a real effect.

The pitch angles derived from the logarithmic part of the two-armed spirals change as function of the color except for NGC 3223 which has a pattern too tight for an accurate estimate. The spirals are systematically more open measured at longer wavelength (i.e. K′) than in bluer bands as seen in Table 5. The radial variation of θ_2 in the V and K′ bands is shown in Fig. 15. This behavior is expected for a trailing density wave inside CR due to the increase of $|\Omega(r) - \Omega_{\mathrm{p}}|$ towards ILR which causes material to float faster through the arms at smaller radii. The change of pitch angle with color strongly suggests the presence of a density wave as material arms would not show a similar effect. The trend is likely due to a combined effect of displacements of both dust and young objects where the latter is less important (Yuan & Grosbøl 1981). The two effects cannot be separated (e.g. using a reddening free color index for stars like Q) since stars and dust are intermixed (Witt et al. 1992). The radius of CR could be determined if one clearly would observe the dust lanes change their location relative to the spiral arms. Such crossing of dust lanes is not seen. Although a systematic difference of the pitch angles as function of color is observed, one cannot use this fact to reliably extrapolate to the location of CR since the nature and absolute size of the phase offset in the different colors are unclear.

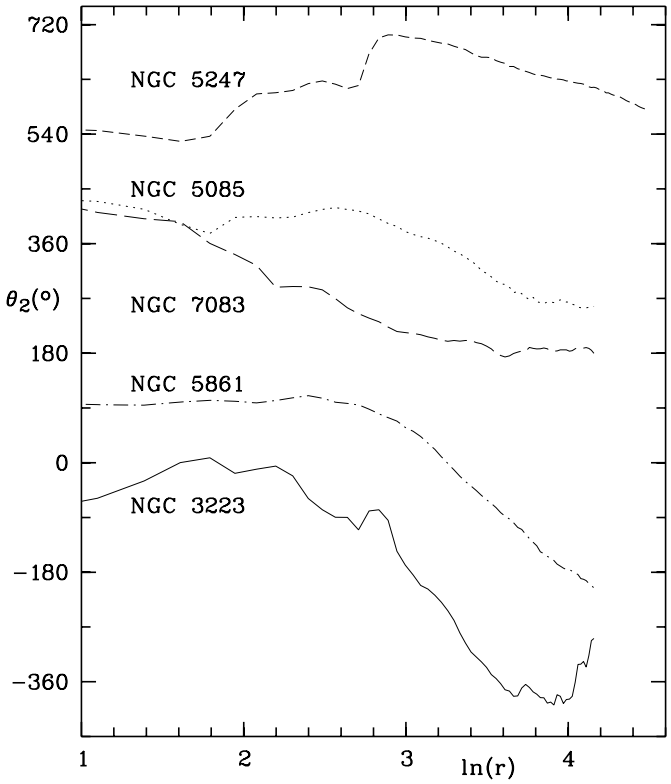

Fig. 14. Phase θ_2 as function of $\ln(r)$ for the galaxies in the K′ band.

Table 5. Average pitch angle i_2 of the main two-armed spiral as measured in different colors for the five galaxies. Estimated error Δ of the angles and the radial range used are listed.

	Pitch angle i_2					
Galaxy	K′	I	V	B	Δ	range
NGC 3223	-8.°8	-9.°4	-8.°8	-8.°7	0.°5	25-36″
NGC 5085	-17.°4	-13.°0	-11.°7	-10.°9	0.°5	25-40″
NGC 5247	-34.°1	-31.°8	-29.°9	-27.°4	0.°7	30-50″
NGC 5861	-12.°4	-11.°8	-11.°9	-	0.°5	20-35″
NGC 7083	-22.°1	-20.°3	-17.°6	-15.°0	1.°0	11-18″

It is expected that major dynamic resonances (i.e. ILR, 4:1, CR, -4:1 and OLR) will either limit to the extend of the spirals or give raise to morphological changes if the pattern exists for several revolutions. A weak density wave perturbation can exist between ILR and OLR (see e.g. Bertin et al. 1989a,b) while non-linear effects would make it difficult to have a strong wave outside the 4:1 resonance (Contopoulos & Grosbøl 1988). Comparing the extend of the strong, two-armed spirals in the galaxies with their angular rotation curves, the best agreement was in all cases achieved assuming that the spiral starts just outside the ILR and terminates around 4:1 while weaker multi-armed spirals extend further. In some cases, it would be marginally possible to

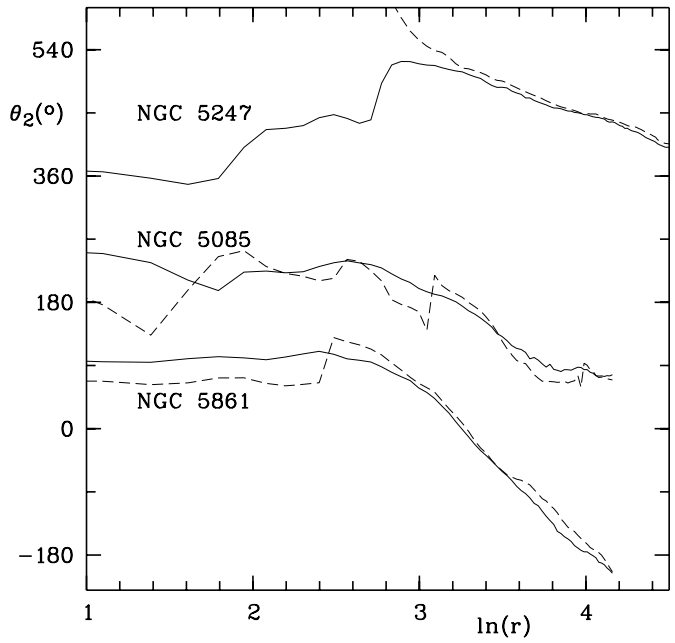

Fig. 15. Radial variation of the phase θ_2 of the spirals for NGC 5085, NGC 5247, and NGC 5861 in V (– –) and K′(—).

Table 6. Average relative amplitudes of oval distortions and inner part of the main two-armed spiral in the galaxies together with the estimated radii of their main resonances. The pattern speed $\Omega_{\rm p}$ estimated for a density wave is given in km s^{-1} kpc^{-1}.

	$< a_2 >$					
Galaxy	bar	spiral	$r_{\rm ILR}$	$r_{4:1}$	$r_{\rm CR}$	$\Omega_{\rm p}$
NGC 3223	0.01	0.07	14″	39″	64″	26.0
NGC 5085	0.10	0.17	12″	41″	77″	18.9
NGC 5247	0.06	-	19″	68″	104″	20.3
NGC 5861	0.07	0.13	9″	43″	84″	17.9
NGC 7083	0.02	0.12	8″	26″	44″	26.2

associate CR and OLR to these location although the appearance of the arms is not similar to that expected from simulation (Patsis et al. 1997). Pattern speeds and locations of the major resonances are listed in Table 6. It is noted that the two Sb galaxies both have a higher pattern speed $\Omega_{\rm p}$ ≈26 km s^{-1} kpc^{-1} than the three Sc galaxies which all have values around 19 km s^{-1} kpc^{-1}. The sample is too small and has other correlation (e.g. linear size) to make this difference significant.

The rotation curves are based on the axisymmetric decomposition of the K′ maps and are therefore not dependent on the spiral pattern observed in the galaxies. The agreement between the location of resonances and the extend of the spiral arms suggests that the spiral pattern exists long enough for it to respond to the axisymmetric gravitational field. This would not necessarily be the case for a single wave package traveling through the disk.

Three of the galaxies have significant oval distortions with relative amplitudes of 6-10% in their central regions whereas the amplitudes for NGC 3223 and NGC 7083 are less then 2%. It is noted that the two galaxies without significant oval distortions have more centrally condensed bulge regions than the galaxies with weak bars. This agrees with Norman et al. (1996) who find that bars may be dissolved in models with sufficient central mass concentration.

The amplitudes a_2 of main two-armed spiral pattern are given in Table 6 where the values for the inner parts are listed. The optically flocculent galaxies in the sample have a_2 values similar to those of the grand design spirals. In several cases, a_2 increases significantly just inside the radius where a_4/a_2 has a local maximum. This increase is probably due to additional contribution of light from young objects in the arm regions and does not reflect a real increase in the amplitude of the underlying density wave. Some of the galaxies show a decrease of a_2 in the 4:1 resonance region which is expected for strong spiral perturbations (Contopoulos & Grosbøl 1988). The density perturbation cannot be estimated reliably without correcting the surface brightness variation in K′ for population effects. Further, the low surface brightness in the interarm regions makes the estimated amplitude uncertain at larger radii. The a_2 amplitudes are consistent with a marginal non-linear density perturbation (Grosbøl 1993) considering that they are overestimated due to light from young objects in the arms.

The m=1 component in the galaxies is generally less than 3% with exception of peaks at 10-15% in the outer parts of NGC 5861 and NGC 7083. The phase of the m=1 component is not well correlated with that of the main two-armed pattern.

Weak spirals in the bulge regions are observed in most of the galaxies. They are better seen on the (V-K′) maps suggesting them to be associated to dust and gas. Dust lanes in the nuclear regions of spiral galaxies were first noted by Baade (1958) for M 31 (see also Johnson 1961; Johnson & Hanna 1972). Their presence would lead to a wrong estimate of the radial extend of stellar spirals arms in galaxies observed in visual bands. They seem to extend the dust lanes of the main spiral inwards across the ILR however with a different shape. The resolution in the inner regions is unfortunately not good enough to measure the phase shift predicted by the density wave theory (Lin & Lau 1979).

The increasing radial wavelength of the spirals close to ILR is in agreement with the long waved solution for trailing waves in the Lin-Shu dispersion relation while a decrease would be expected for the short waved branch. If the spiral pattern is associated to the long waved branch, it would have an outgoing group velocity. A possible scenario would be a spiral driven by an oval distortion in the center (Schwarz 1981). The central bar could be fast rotating with its CR coupled to the ILR of the spiral pattern (Sellwood & Sparke 1988). The outgoing wave package would be damped at the 4:1 resonance by non-linear effects (Contopoulos & Grosbøl 1988).

6. Conclusion

The five spiral galaxies analyzed in this paper show several common properties. The general conclusion can be summarized as follows:

1. Spiral arm morphology based on optical studies, is strongly biased by attenuation of dust in the galaxies and does not reflect the perturbation in the old stellar disk population. Gaseous and stellar disks are decoupled in the optically flocculent galaxies studied here and show very different morphologies.
2. The central surface brightness distribution of the galaxies in K′ could not be explained by a single spherical bulge component but required an additional exponential disk with projection parameters similar to that of the main disk.
3. The scale length of the main exponential disk measured in the interarm regions is significantly smaller than the one estimated for the spiral arms. The sharpness of many knots in K′ maps and their location in the arm regions indicate that they are kinematically young. This suggests that the light from young objects contributes a significant fraction of the K′ luminosity in the arms regions.
4. The main two-armed spiral is tighter when measured in bluer colors than that estimated on the K′ maps. This strongly indicates the presence of a spiral density wave in the galaxies.
5. Comparing major morphological features of the main spiral pattern (e.g. the radial extend of the strong symmetric spiral, presence of interarm spurs and bifurcation of arms) with the angular velocity curve, the best agreement was found assuming that the strong two-armed spiral pattern exists between ILR and 4:1 with weaker extensions outwards.
6. The frequency of central oval distortions observed in K′ is higher than that seen on bluer images. Two of the four galaxies classified as ordinary spirals showed a significant central perturbation.
7. The outer parts of the strong arms are well fitted with a logarithmic spiral but their radial wavelength increases in the inner region close to the ILR.
8. Dust spirals are frequently observed in the central parts inside the main spiral pattern. In some cases, weak inner spirals in the disk population were identified.
9. The pattern speed estimated for the Sb galaxies in the sample is higher than the average for the Sc galaxies.

The current paper presents a detailed analysis of the spiral pattern in five galaxies. An accurate account of the shape and amplitude of spiral arms will be made when a detailed correction for young objects in the K′ maps can be applied. This will make a through comparison between observed spiral patterns and prediction based on the density wave theory possible.

Acknowledgements. We are very grateful for numerous fruitful discussions with Prof. G. Contopoulos. It is also a pleasure to thank the referee, Prof. D.L. Block, for valuable comments. All image processing was done with the ESO-MIDAS system while mathematical formulae were checked using the Maple V package.

References

Aaronson, M., Huchra, J., Mould, J.R., Tully, R.B., Fisher, J.R., van Woerden, H., Goss, W.M., Chamaraux, P., et al., 1982, ApJS, 50, 241
Abramowitz, M., Stegun, I., 1965, *Handbook of Mathematical Functions*, Dover, New York
Baade, W., 1958, IAU Sym. 5, Ed. N.G. Roman, Cambridge, 1
Bertin, G., Lin, C.C., Lowe, S.A., Thurstans, R.P., 1989a, ApJ, 388, 78
Bertin, G., Lin, C.C., Lowe, S.A., Thurstans, R.P., 1989b, ApJ, 388, 104
Bessell, M.S., Brett, J.M., 1998, PASP, 100, 1134
Binney, J., Tremaine, S., 1987, *Galactic Dynamics*, Princeton Univ. Press, Princeton
Block, D.L., 1996, *New Extragalactic Perspectives in the New South Africa*, Eds. D.L. Block and J.Mayo Greenberg, Kluwer, ASSL 209, 1
Block, D.L., Bertin,G., Stockton, A. et al., 1994, A&A, 288, 365
Block, D.L., Elmegreen, B.G., Wainscoat, R.J., 1996, Nat, 381, 674
Block, D.L., Wainscoat, R.J., 1991, Nat, 353, 48
Bottema, R., 1997, A&A, 328, 517
Byun, Y.I., Freeman, K.C., Kylafis, N.D., 1994, ApJ, 432, 114
Canzian, B., Allen, R.J., 1997, ApJ, 479, 723
Charlot, S., Worthey, G., Bressan, A., 1996, ApJ, 457, 625
Chiosi, C., Vallenari, A., 1996, *Spiral Galaxies in the Near-IR*, ESO Astrophys. Symp., Eds. D. Minniti and H.-W. Rix, Springer, Berlin, 63
Contopoulos, C., Grosbøl, P., 1986, A&A, 155, 11
Contopoulos, C., Grosbøl, P., 1988, A&A, 197, 83
Courteau, S., de Jong, R.S., Broeils, A.H., 1996, ApJ, 457, 73L
Danver, C.-G., 1942, Ann. Obs. Lund No. 10
de Jong, R.S., 1996, A&AS, 118, 557
de Vaucouleurs, G., de Vaucouleurs, A., Cowien, Jr.,H.G. et al., 1991, *Third reference catalogue of bright galaxies* (RC3), Springer, New York
de Vaucouleurs, A., Longo, G., 1988, Monographs in Astronomy No. 5, Austin, Texas
Elmegreen, B.G., Block, D.L., 1998, in preparation
Elmegreen, D.M., Elmegreen, B.G., 1982, MNRAS, 201, 1021
Elmegreen, D.M., Elmegreen, B.G., 1987, ApJ, 314, 3
Fisher, J.R., Tully, R.B., 1981, ApJS, 47, 139
Freeman, K.C., 1970, ApJ, 160, 811
Grosbøl, P., 1993, PASP, 105, 651
Héraudeau, Ph., Simien, F., Mamon, G.A., 1996, *Spiral Galaxies in the Near-IR*, ESO Astrophys. Symp., Eds. D. Minniti and H.-W. Rix, Springer, Berlin, 235
Johnson, H.M., 1961, ApJ, 133, 309
Johnson, H.M., Hanna, M.M., 1972, ApJ, 174, L71
Kent, S.M., 1986, AJ, 91, 1301
Landolt, A.U., 1992, AJ, 104, 340
Lin, C.C., Shu, F.H., 1964, ApJ, 140, 646
Lin, C.C., Lau, Y.Y., 1979, Studies in Applied Math., 60, 97
Longo, G., de Vaucouleurs, A., 1983, Monographs in Astronomy No. 3, Austin, Texas
Norman, C.A., Sellwood, J.A., Hasan, H., 1996, ApJ, 462, 114
Patsis, P.A., Contopoulos, G., Grosbøl, P., 1991, A&A, 243, 373
Patsis, P.A., Grosbøl, P., Hiotelis, N., 1997, A&A, 323, 762
Quillen, A.C., 1996, *Spiral Galaxies in the Near-IR*, ESO Astrophys. Symp., Eds. D. Minniti and H.-W. Rix, Springer, Berlin, 157
Rix, H.-W., 1993, PASP, 105, 999
Rix, H.-W., Rieke, M.J., 1993, ApJ 418, 123
Rubin, V.C., Ford, W.K.Jr., Thonnard, N., 1982, ApJ, 261, 439

Sandage, A., Tammann, G.A., 1981, *A Revised Shapley-Ames Catalog of Bright Galaxies* (RSC), Carnegie Inst. Wash. Pub. no. 635, Washington, D.C.
Schempp, W.V., 1982, ApJ, 258, 96
Schwarz, M.P., 1981, ApJ, 247, 77
Schweizer, F., 1976, ApJS, 31, 313
Scorza, C. Bender, R., 1995, A&A, 293, 20
Seifert, W., Scorza, C., 1996, A&A, 310, 75
Sellwood, J.A., Sparke, L.S., 1988, MNRAS, 231, 25
Toomre, A. 1969, ApJ, 158, 899
Toomre, A., 1981, in *The structure and evolution of normal galaxies*, Eds. S.M.Fall and D.Lynden-Bell, Cambridge Univ. Press, Cambridge, 111
van der Bosch, P.C., Ferrarese, L., Ford, H.C., Jaffe, W., O'Connell, R.W. 1994, AJ, 108, 1579
Visser, H.C.D. 1980, A&A, 88, 159
Wainscoat, R.J., Cowie, L.L. 1992, AJ, 103, 332
Wielen, R., 1977, A&A, 60, 263
Witt, A.N., Thronson, H.A., Capuano, J.M.,Jr., 1992, ApJ, 393, 611
Yuan, C., Grosbøl 1981, ApJ 243, 432